Single-Molecule Microscopy

Deutsche Ausgabe: DOI: 10.1002/ange.201505138
Internationale Ausgabe: DOI: 10.1002/anie.201505138

Multicolor Caged dSTORM Resolves the Ultrastructure of Synaptic Vesicles in the Brain

Martin Lehmann, Benjamin Gottschalk, Dmytro Puchkov, Peter Schmieder, Sergej Schwagerus, Christian P. R. Hackenberger, Volker Haucke, and Jan Schmoranzer**

Abstract: *The precision of single-molecule localization-based super-resolution microscopy, including dSTORM, critically depends on the number of detected photons per localization. Recently, reductive caging of fluorescent dyes followed by UV-induced recovery in oxidative buffer systems was used to increase the photon yield and thereby the localization precision in single-color dSTORM. By screening 39 dyes for their fluorescence caging and recovery kinetics, we identify novel dyes that are suitable for multicolor caged dSTORM. Using a dye pair suited for registration error-free multicolor dSTORM based on spectral demixing (SD), a multicolor localization precision below 15 nm was achieved. Caged SD-dSTORM can resolve the ultrastructure of single 40 nm synaptic vesicles in brain sections similar to images obtained by immuno-electron microscopy, yet with much improved label density in two independent channels.*

The localization precision of single-molecule based super-resolution imaging methods, including (d)STORM, (f)PALM, and GSDIM, critically depends on the number of detected photons per single molecule.[1–5] Recently, reductive caging of fluorescent organic dyes by $NaBH_4$ and subsequent UV-induced fluorescence recovery in buffer systems that prolong the fluorescent ON state increased photon counts and single color localization precision to below 10 nm for samples labeled in vitro.[6] Although several spectrally distinct dyes were identified for reductive caging,[6–8] no multicolor caged (d)STORM at such high resolutions, in particular in neuronal samples, has been demonstrated so far.

[*] M. Lehmann,[+] B. Gottschalk,[+] D. Puchkov, P. Schmieder, S. Schwagerus, C. P. R. Hackenberger, V. Haucke, J. Schmoranzer
Leibniz Institut für Molekulare Pharmakologie (FMP)
Robert-Roessle-Strasse 10, 13125 Berlin (Germany)
E-mail: martin.lehmann@fu-berlin.de
jan.schmoranzer@fu-berlin.de
M. Lehmann,[+] V. Haucke, J. Schmoranzer
Freie Universität Berlin, Department of Biochemistry
Takustrasse 6, 14195 Berlin (Germany)
C. P. R. Hackenberger
Humboldt Universität zu Berlin, Department of Chemistry
Brook-Taylor-Strasse. 2, 12489 Berlin (Germany)
J. Schmoranzer
Charité - Universitätsmedizin Berlin, Charité Campus Mitte
Virchowweg 6, 10117 Berlin (Germany)
[+] These authors contributed equally to this work.
Supporting information and ORCID(s) from the author(s) for this article are available on the WWW under http://dx.doi.org/10.1002/anie.201505138.

To overcome common limitations in multicolor super-resolution applications, including channel crosstalk and registration errors, we previously introduced spectral demixing (SD)-based dSTORM.[9] Similar to other approaches SD-dSTORM uses a split-view detection to separate spectrally overlapping fluorophores based on intensity ratios.[10,11] However, SD-dSTORM uses a custom algorithm that avoids registration errors and is thus particularly suited for precise multicolor super-resolution imaging.[12]

To identify spectrally suitable dyes for multicolor caged dSTORM, we conducted a screen probing the reduction kinetics of 39 commercially available dyes, comprising rhodamines, oxazines, cyanines, coumarines, and carbopyronine dyes that should be efficiently reduced by $NaBH_4$ according to their reduction potential (E_{red} $NaBH_4$ vs. SCE = −1.48 V).[6,7,13,14] For efficient screening, the dye-labeled antibodies were immobilized on a 96-well plate and the fluorescence decay was measured after addition of 10 mM $NaBH_4$ as a reducing agent (Figure 1a). Out of the 39 dyes tested, 23 were caged efficiently with a half-life below 1000 s (Supporting Information, Figure S1). Although the caging efficiency of most cyanine and rhodamine dyes was high (half-time < 1000 s), reduction did not correlate with the dye class alone (Supporting Information, Figure S1) or with their reduction potentials.[13] For example, some structurally similar rhodamine dyes (Atto488, Atto514, and Atto532) were efficiently caged while other rhodamine dyes (AF514, AF568, Texas Red, and AF594) were not. The reduction of rhodamines was analyzed in more detail for Atto488 by comparative $^1H/^{13}C$ NMR spectroscopy before and after $NaBH_4$ reduction revealing that the hydride attack occurs at the central carbon atom (C12) of the xanthene system (Figure 1c; Supporting Information, Figure S2). This reduction shortens the conjugated π-system, thus drastically decreasing fluorescence, which is in accordance with previous reports on rhodamines.[8,15]

By comparing the chemical structures of the efficiently caged dyes (half-life 100–550 s) with the uncagable dyes (half-time > 1000 s), we observed that the electronic nature of the fluorophore substituents greatly influence the caging efficiency (Supporting Information, Figure S1). Specifically, two electron-withdrawing SO_3^--substituents at the conjugated system of the rhodamine dyes AF488, Atto488, Atto514, Atto532, and AF546 resulted in efficient reductive caging with half-lives below 550 s. In contrast, other electron-withdrawing substituents such as the carboxyl group present in AF488, or the CH_2CF_3-substituent present in Atto514, did not accelerate the reduction kinetics significantly in comparison to Atto488. Slower caging rates (half-life > 1000–10000 s)

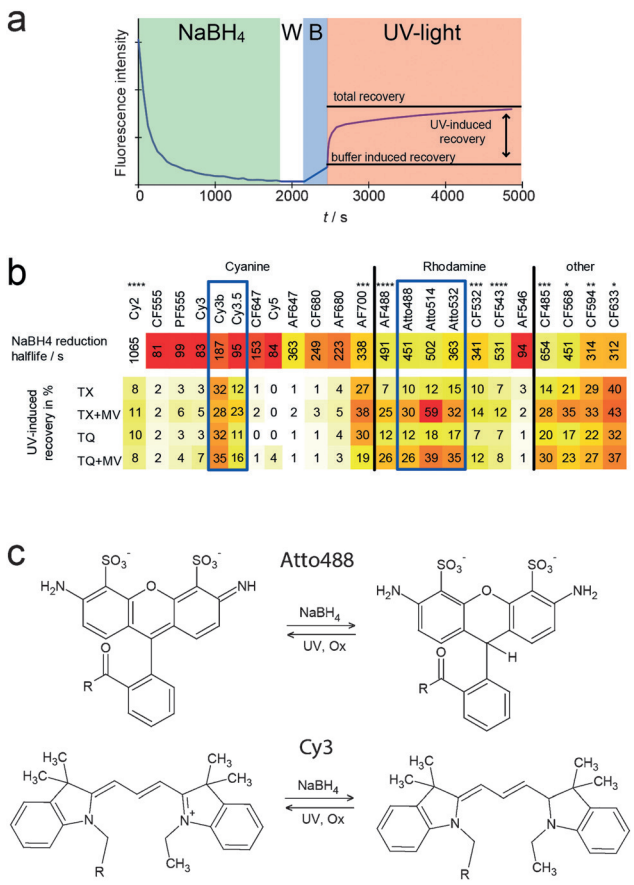

Figure 1. Screening dyes for $NaBH_4$ caging and uncaging kinetics. a) Example of the fluorescence time course of CF568-labeled antibodies during reduction with 10 mM $NaBH_4$ (green), washing (W, white), addition of imaging buffer (B, blue) and UV-induced recovery (pink). b) Fluorescence half-life after $NaBH_4$ reduction and UV-induced recovery of dyes in buffers containing combinations of trolox (TX), methylviologen (MV), and trolox-quinone (TQ). The color scale ranges from red (fast caging/high recovery) to white (slow caging/low recovery) of the indicated dyes. Additional exclusion criteria as assessed by microscopic evaluation are indicated: * low efficiency of uncaging, ** low efficiency of UV activation (405 nm), *** faint blinking, **** activated by excitation laser. Blue boxes mark spectrally suitable candidates for caged SD-dSTORM. (c) Chemical structures of Atto488 (top) as determined by NMR and Cy3 (bottom) before and after reduction.

were observed with larger rhodamine systems (AF514, AF568, AF594, and Texas Red) containing electron-donating alkyl-groups substituents. In contrast, the electron-deficient trichloro-substituted rhodamine system of AF546 was efficiently reduced (half-life = 450 s). The cyanine dyes Cy3 and Cy5 were efficiently caged as previously reported,[6,7] as expected by the reduction potentials (Figure 1 c).[14] In contrast, Cy2 showed a significantly slower reduction rate (half-life > 1000 s). The reported reduction efficiencies of the investigated dyes (Supporting Information, Figure S1 a) could serve as a basis for future studies investigating the effects of specific substituents on caging efficiencies.

Efficiently caged dyes were further screened for their recovery properties in imaging buffers containing different combinations of chemical redox systems, fluorescence triplet state quenchers, and an oxygen scavenging system (Figure 1 b).[6,16–18] Most rhodamine dyes tested were efficiently recovered by UV light in the presence of the oxidizers methylviologen and trolox, with the exception of AF546. Generally, the recovery rate of reduced cyanine dyes was low, even in the presence of the photosensitizer riboflavin. From the cyanine dyes, Cy3b displayed the most efficient UV-induced recovery. The more efficient light-induced recovery (oxidation) of rhodamine dyes compared to cyanine dyes could be explained by a lower free enthalpy change for charge separation of an excited fluorophore for photoinduced electron transfer processes, according to the Rehm–Weller equation[13,17] (Supporting Information).

The recovery of the cyanine dyes may be increased by low amounts of stronger oxidizers such as Fenton's reagent or ammonium persulfate.[7,8] Alternative triplet-state quenchers, for example systems based on ROXS,[17] self-healing fluorophores,[19] or the physical triplet state quencher Ni^{2+},[20] could further increase the photon yields of caged dSTORM. Furthermore, the novel cagable dyes could be used to multiplex recently introduced sequential labeling procedures for dSTORM that rely on $NaBH_4$-based reduction and subsequent photodestruction.[21,22] Finally, some of the identified non-cagable dyes (Atto647N, Chromeo493) might serve as photoactivators for dyes with low recovery,[23] or as spectrally separate wide-field reference to expand the experimental capabilities of caged SD-dSTORM in biological applications.

From the 14 dyes that were both caged and recovered efficiently, we selected the spectrally overlapping rhodamines (Atto488, 514, 532) and the cyanines (Cy3b, Cy3.5) as candidates to perform caged SD-dSTORM. To investigate the performance of the dyes (caging, recovery, brightness), we conducted single-color caged dSTORM of immunolabeled microtubules (MTs). Caged dSTORM images displayed clear MT filaments with high labeling densities, defined crossings, typical widths of 49-55 nm (Figure 2 a), and occasional occurrence of double-peaked transverse intensity profiles (Supporting Information, Figure S3), consistent with previous results on immunolabeled MTs under similar conditions.[6,23,24] To optimize the imaging buffer conditions for caged dSTORM, we independently determined the photon yields (from single molecule signals) and the localization precisions from the full width at half maximum (FWHM) of the localization distribution, using combinations of the triplet stage quencher Trolox (TX) or Trolox-Quinone (TQ), with or without the oxidizer methylviologen (MV) (Figure 2 b,c, Supporting Information). For the Atto and cyanine dyes, TQ + MV and TX + MV significantly improved both the photon yield and the FWHM compared to AF647. The final image resolution can be estimated from the precision of single molecule localization (FWHM), the drift correction, and localization density (Nyquist resolution). Taking all these into account, caged dSTORM imaging optimally achieves an image resolution of 16–19 nm for the Atto dyes, and 24–29 nm for Cy3b and Cy3.5, while dSTORM has an image resolution of 25 nm using AF647 (Supporting Information, Table S4). The superior image resolution of the caged Atto dyes was confirmed by an independent analysis using Fourier ring correlation (Supporting Information, Table S4).[25] By using

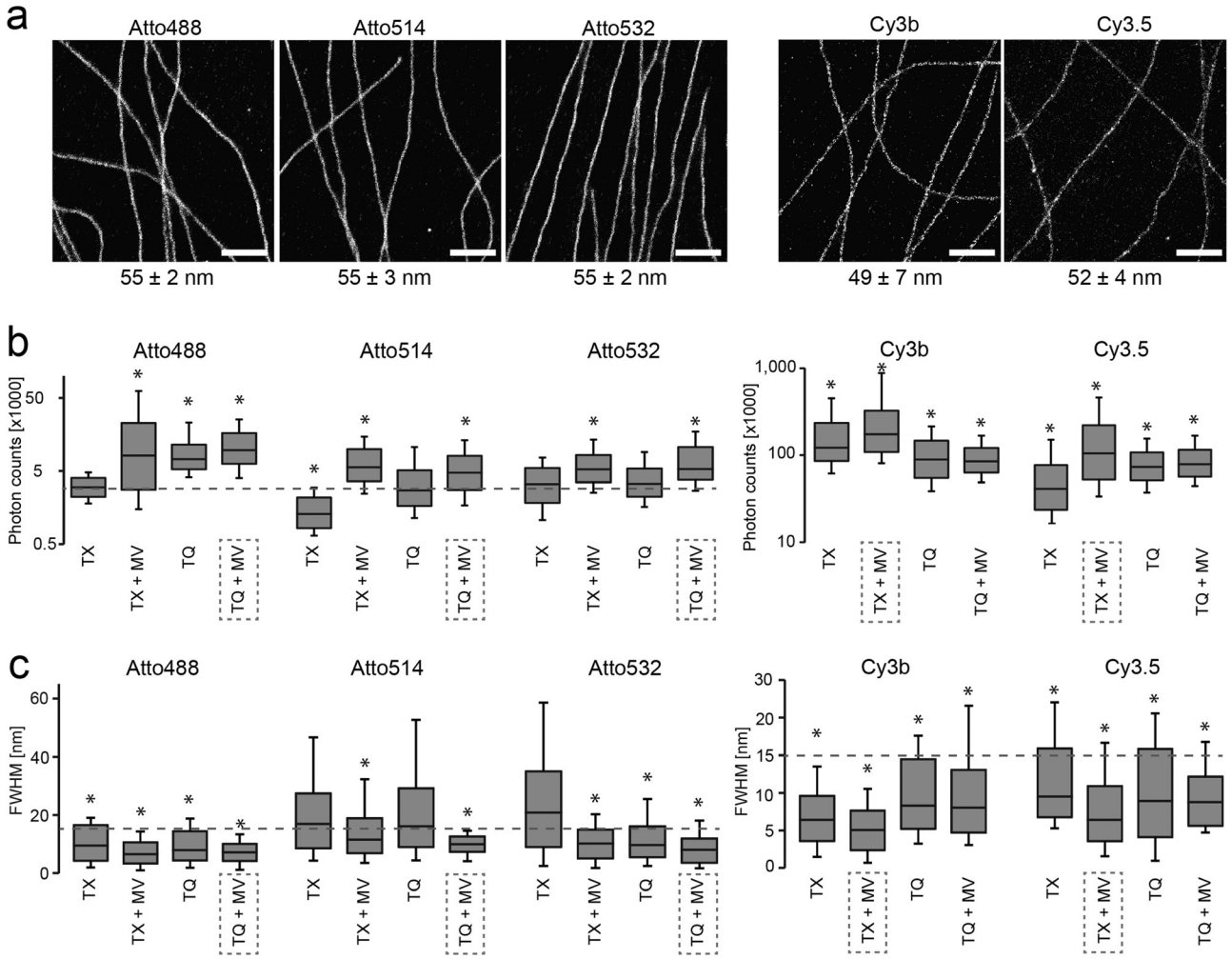

Figure 2. Characterization of caged dSTORM using Atto488, Atto514, Atto532, Cy3b, and Cy3.5. a) NIH-3T3 cells were immunolabeled for MTs with indicated dyes and imaged by caged dSTORM in presence of TQ + MV for Atto dyes and TX + MV for Cy3b and Cy3.5. The average width of the MTs (± StDev) was determined from FWHM of 10 representative profiles. b, c) Single-molecule photon counts (b) and localization precisions (FWHM) (c) in different buffers measured from single antibodies labeled with indicated dyes. Dotted lines mark the measured photon counts and localization precision of AF647 using dSTORM. Dotted boxes mark the optimal buffer conditions used. * indicates significance compared to AF647 ($p < 0.001$, Wilcoxon–Mann–Whitney test). Scale bars: 1 μm.

an alternative excitation (543 nm vs. 568 nm) and optimizing recovery (see above), the performance of Cy3b and Cy3.5, that indeed offer very high photon counts, could be improved.

Since Atto488 and Atto532 showed both high localization precision and recovery, in contrast to the cyanine dyes, we used them in multicolor caged dSTORM based on spectral demixing (SD). By optimizing the dichroic-based emission splitter and the color assignment filters for spectral demixing, we achieved low crosstalk (2–4%), perfect registration of dual-labeled MTs, and a localization precision (FWHM) of around 15 nm (Supporting Information, Figure S4). We then performed caged SD-dSTORM on immunolabeled cells using Atto488 and Atto532. The sub-diffraction widths of MTs (Atto488: 59 ± 7 nm, Atto532: 58 ± 7 nm) and the characteristic ring-like ultrastructure of spherical clathrin-coated pits (CCPs) (Atto488: 159 ± 29 nm, Atto532: 169 ± 23) agree well with the single-color measurements (Figure 2a), and with the previously measured dimensions of these structures using immunolabeling.[23]

Proper neurotransmission relies upon the precise spatial organization of densely packed synaptic vesicles (SVs), and upon the machinery for their exocytosis and endocytosis within the presynaptic terminal. Transmission electron microscopy (TEM) can resolve the membrane boundaries of densely packed single SVs (35 nm diameter) and clathrin-coated vesicles (CCVs, 50 nm diameter), but is not suitable for revealing the molecular identity of multiple components of single SVs. Previously, stimulated emission depletion (STED) microscopy was used to resolve diffraction-limited (about 66 nm) puncta in hippocampal neurons that were interpreted as mobile single SVs.[26] However, the ultrastructure of single SVs or CCVs has not been resolved thus far using fluorescence microscopy methods. To fill in this gap, we analyzed whether caged SD-dSTORM is able to resolve distinct SV proteins and separate these from endocytic intermediates within the presynaptic terminal.

We first used TEM to ascertain that presynaptic terminals, including the SV membranes, remained morphologically

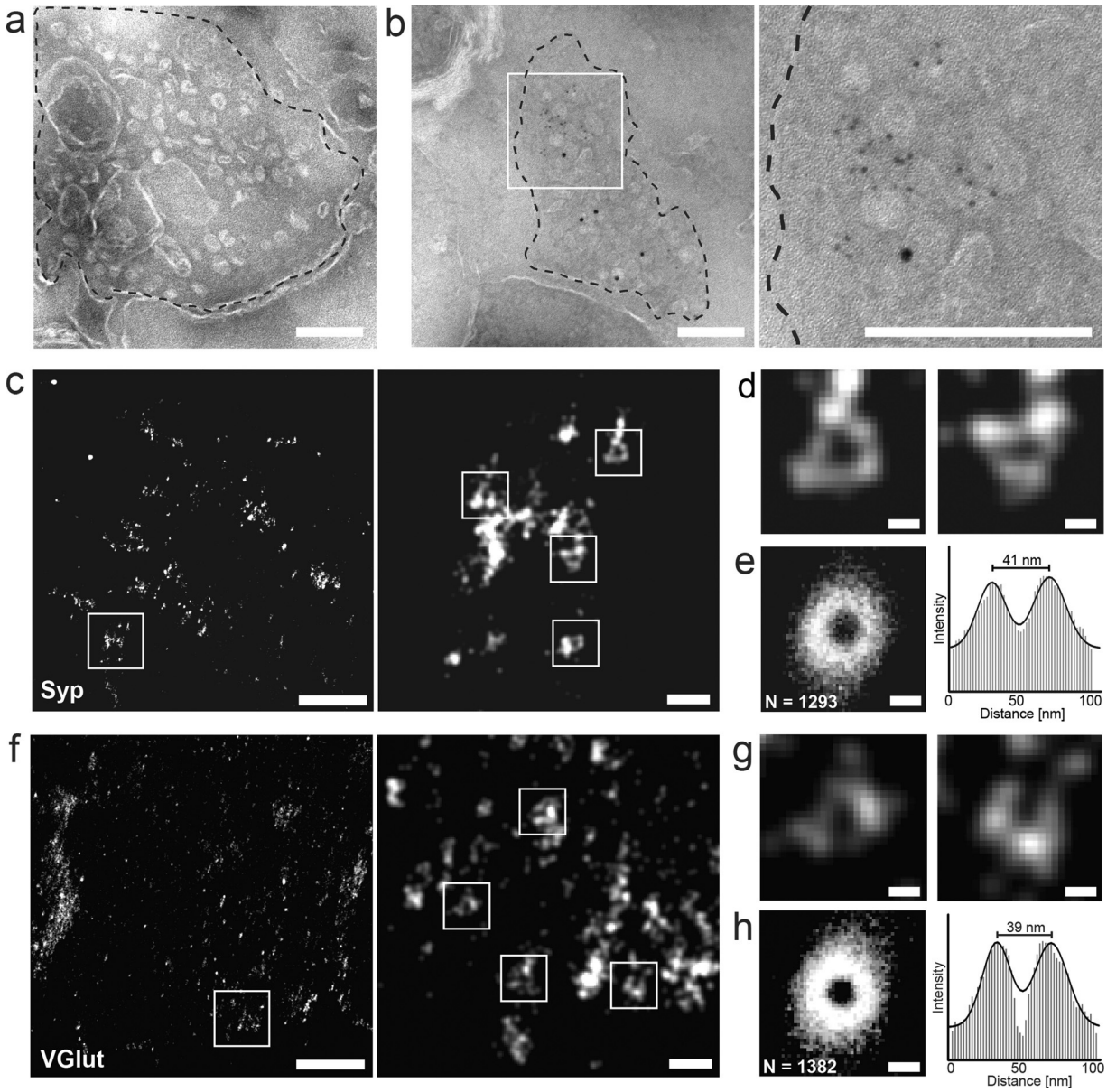

Figure 3. TEM and caged dSTORM imaging of presynaptic terminals. a, b) TEM images of 80 nm cryosections of mouse brain (a) treated with 10 mM $NaBH_4$ for 30 min or (b) immunolabeled for CHC (6 nm gold) and VGlut (12 nm gold). The presynaptic areas are marked with dotted lines. c, f) Caged dSTORM and enlarged area of 150 nm cryosection of mouse brain immunolabeled for Syp (c–e) and VGlut (f–h) using Atto488. (c, f) Boxed region of large scale view (left) is enlarged to the right showing single ring-like structures (small boxes). (d, g) Example regions showing ring-like structures. (e, h) Superimposition of localizations from indicated numbers of selected areas (N) with ring-like structures and the corresponding intensity profile. Scale bars: a, b) 200 nm; c, f) left: 1 μm, right: 100 nm; d, e, g, h) 20 nm.

intact within ultra-thin brain cryosections[27] following the caging procedure (Figure 3). Immunogold TEM of the brain sections confirmed that two synaptic proteins, the vesicular glutamate transporter 1 (VGlut1) and clathrin, were accessible to antibodies but displayed typical sparse labeling density. We then studied the synaptic ultrastructure by single-color caged dSTORM of two SV membrane proteins, synaptophysin (Syp) and VGlut1. In both cases, we observed heterogeneous clusters of about 1 μm in width, the characteristic size of presynaptic hippocampal boutons. Within these synaptic boutons, we frequently observed partially labeled ring-like structures. The superimposition of over 1000 of these structures revealed clear rings with diameters consistent with the known diameter of SVs from TEM studies. These data demonstrate that the ultrastructure of single SVs within densely labeled brain sections can be resolved using caged dSTORM.

Next, we investigated whether dual-color caged SD-dSTORM allows us to assess the localization of single SVs and endocytic intermediates undergoing recycling to replenish SV pools. We labeled three SV membrane proteins, namely VGlut1, Syp and synaptobrevin2 (Syb2), and clathrin heavy chain (CHC), as markers for endocytic intermediates using specific antibodies (Figure 4; Supporting Information,

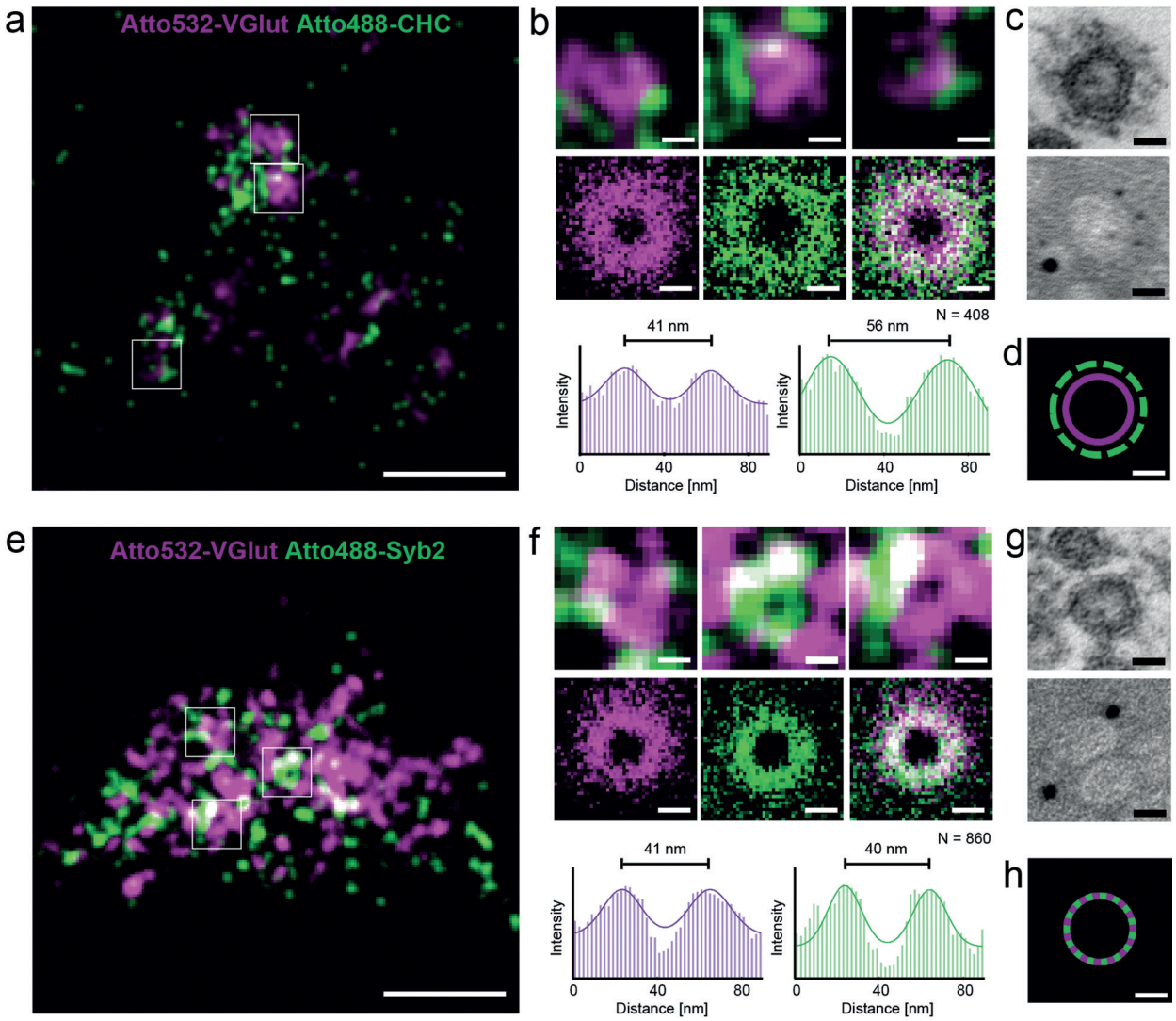

Figure 4. Caged SD-dSTORM imaging of presynaptic terminals in 150 nm cryosections of mouse brain immunolabeled for a, b) VGlut/clathrin and e, f) VGlut/Syb2 using indicated dyes. a, e) Representative areas. b, f) Top: enlarged regions from (a, e). Center: Superimpositions of localizations from N selected regions. Bottom: Intensity profiles from superimpositions for indicated colors. c, g) TEM (top) and immuno TEM for CHC (6 nm gold, small particles) and VGlut (12 nm gold, big particles) of single CCV (c) and SV (d) (bottom). d, h) Representation of the indicated membrane and coat markers in a single CCV (d) and SV (h). Scale bars: a, e) 250 nm; b–d, f–h) 20 nm.

Figure S5). Within synapses, we observe partially labeled ring-like structures in all three color combinations. Superimposition of over 400 ring-like structures revealed an average ring diameter of 41 nm for VGlut and 56 nm for clathrin, consistent with the volume projections of antibody decorated spherical SVs and CCV that are about 35 nm and 50 nm in diameter in TEM, respectively (Figure 4). The ring-like structures and superimposition diameters of Syb2 (40 nm) and Syp (39 nm) were very similar to that of VGlut. These data thus demonstrate that dual-color caged SD-dSTORM on ultra-thin brain sections provided sufficient label density and experimental resolution to detect the ultrastructure of SVs and endocytic intermediates in the presynaptic terminal. Traditional immunogold TEM is challenged by low antigen-labelling efficacy owing to the large size of covalently bound colloidal gold particles (Figures 3, 4), or artifacts associated with silver/gold enhancement. In contrast, caged dSTORM uses standard immunolabeling on intact cells with improved label densities and larger fields of view, offering ultrastructural resolution as an alternative for TEM, especially for multicolor imaging.

Furthermore, we provide visual evidence of the biochemical observation that SV proteins are the main cargo of presynaptic endocytic CCV[28,29] and are consistent with a role for clathrin in SV reformation.[30,31] By using a combination of proteomics and quantitative western blotting, the average protein contents of single SV have been determined in synaptosome preparations containing many hundreds of SVs.[32] Our data now offer a first glance at the distribution of SV membrane proteins on the single SV level in brain. Therefore, this approach could serve as a starting point to analyze the proteins contents of individual SVs. Improving the label density of endogenous proteins, that is, by using smaller probes (apatameres,[33] nanobodies),[34] will help to

gain further insights into the composition of distinct compartments or vesicle pools within small central synapses.

By employing registration error-free caged SD-STORM, we present the first data resolving the 40 nm ring-like structure as volume projection of single SVs in mouse brain. As caged SD-dSTORM can be extended to other spectral regions, or to 3D imaging in combination with smaller probes for labeling, we expect this method to be able to resolve the ultrastructure of any densely packed cellular organelles below the diffraction limit of light and thus, serve as a prime alternative to immunogold TEM, yet with much improved label efficiency.

Acknowledgements

We thank Martina Ringling for technical assistance. This work was supported by grants from the German Funding Agency (DFG) (SFB958/Z02 to J.S. and SFB958/A01 to V.H.)

Keywords: electron microscopy · fluorescent probes · immunochemistry · NMR spectroscopy · single-molecule studies

How to cite: *Angew. Chem. Int. Ed.* **2015**, *54*, 13230–13235
Angew. Chem. **2015**, *127*, 13428–13433

[1] E. Betzig, G. H. Patterson, R. Sougrat, O. W. Lindwasser, S. Olenych, J. S. Bonifacino, M. W. Davidson, J. Lippincott-Schwartz, H. F. Hess, *Science* **2006**, *313*, 1642–1645.
[2] S. T. Hess, T. P. K. Girirajan, M. D. Mason, *Biophys. J.* **2006**, *91*, 4258–4272.
[3] M. J. Rust, M. Bates, X. Zhuang, *Nat. Methods* **2006**, *3*, 793–796.
[4] M. Heilemann, S. van de Linde, M. Schüttpelz, R. Kasper, B. Seefeldt, A. Mukherjee, P. Tinnefeld, M. Sauer, *Angew. Chem. Int. Ed.* **2008**, *47*, 6172–6176; *Angew. Chem.* **2008**, *120*, 6266–6271.
[5] A. Egner, C. Geisler, C. von Middendorff, H. Bock, D. Wenzel, R. Medda, M. Andresen, A. C. Stiel, S. Jakobs, C. Eggeling, et al., *Biophys. J.* **2007**, *93*, 3285–3290.
[6] J. C. Vaughan, S. Jia, X. Zhuang, *Nat. Methods* **2012**, *9*, 1181–1184.
[7] K. Kundu, S. F. Knight, N. Willett, S. Lee, W. R. Taylor, N. Murthy, *Angew. Chem. Int. Ed.* **2009**, *48*, 299–303; *Angew. Chem.* **2009**, *121*, 305–309.
[8] L. Carlini, A. Benke, L. Reymond, G. Lukinavičius, S. Manley, *ChemPhysChem* **2014**, *15*, 750–755.
[9] A. Lampe, V. Haucke, S. J. Sigrist, M. Heilemann, J. Schmoranzer, *Biol. Cell* **2012**, *104*, 229–237.
[10] M. Bossi, J. Fölling, V. N. Belov, V. P. Boyarskiy, R. Medda, A. Egner, C. Eggeling, A. Schönle, S. W. Hell, *Nano Lett.* **2008**, *8*, 2463–2468.
[11] D. Baddeley, D. Crossman, S. Rossberger, J. E. Cheyne, J. M. Montgomery, I. D. Jayasinghe, C. Cremer, M. B. Cannell, C. Soeller, PLoS ONE**2011**, 6, e20645.
[12] G. Tadeus, A. Lampe, J. Schmoranzer, *Methods Appl. Fluoresc.* **2015**, DOI: 10.1088/2050-6120/3/3/037001.
[13] S. Doose, H. Neuweiler, M. Sauer, *ChemPhysChem* **2009**, *10*, 1389–1398.
[14] I. H. Stein, S. Capone, J. H. Smit, F. Baumann, T. Cordes, P. Tinnefeld, *ChemPhysChem* **2012**, *13*, 931–937.
[15] S. van de Linde, M. Sauer, *Chem. Soc. Rev.* **2014**, *43*, 1076–1087.
[16] I. Rasnik, S. A. McKinney, T. Ha, *Nat. Methods* **2006**, *3*, 891–893.
[17] J. Vogelsang, R. Kasper, C. Steinhauer, B. Person, M. Heilemann, M. Sauer, P. Tinnefeld, *Angew. Chem. Int. Ed.* **2008**, *47*, 5465–5469; *Angew. Chem.* **2008**, *120*, 5545–5550.
[18] T. Cordes, J. Vogelsang, P. Tinnefeld, *J. Am. Chem. Soc.* **2009**, *131*, 5018–5019.
[19] R. B. Altman, Q. Zheng, Z. Zhou, D. S. Terry, J. D. Warren, S. C. Blanchard, *Nat. Methods* **2012**, *9*, 428–429.
[20] V. Glembockyte, R. Lincoln, G. Cosa, *J. Am. Chem. Soc.* **2015**, *137*, 1116–1122.
[21] C. C. Valley, S. Liu, D. S. Lidke, K. A. Lidke, *PLoS One* **2015**, *10*, e0123941.
[22] J. Tam, G. A. Cordier, J. S. Borbely, Á. S. Álvarez, M. Lakadamyali, *PLoS One* **2014**, *9*, e101772.
[23] M. Bates, B. Huang, G. T. Dempsey, X. Zhuang, *Science* **2007**, *317*, 1749–1753.
[24] U. Endesfelder, S. Malkusch, F. Fricke, M. Heilemann, *Histochem. Cell Biol.* **2014**, *141*, 629–638.
[25] R. P. J. Nieuwenhuizen, K. A. Lidke, M. Bates, D. L. Puig, D. Grünwald, S. Stallinga, B. Rieger, *Nat. Methods* **2013**, *10*, 557–562.
[26] K. I. Willig, S. O. Rizzoli, V. Westphal, R. Jahn, S. W. Hell, *Nature* **2006**, *440*, 935–939.
[27] K. T. Tokuyasu, *J. Cell Biol.* **1973**, *57*, 551–565.
[28] P. R. Maycox, E. Link, A. Reetz, S. A. Morris, R. Jahn, *J. Cell Biol.* **1992**, *118*, 1379–1388.
[29] F. Blondeau, B. Ritter, P. D. Allaire, S. Wasiak, M. Girard, N. K. Hussain, A. Angers, V. Legendre-Guillemin, L. Roy, D. Boismenu, et al., *Proc. Natl. Acad. Sci. USA* **2004**, *101*, 3833–3838.
[30] N. L. Kononenko, D. Puchkov, G. A. Classen, A. M. Walter, A. Pechstein, L. Sawade, N. Kaempf, T. Trimbuch, D. Lorenz, C. Rosenmund, et al., *Neuron* **2014**, *82*, 981–988.
[31] S. Watanabe, T. Trimbuch, M. Camacho-Pérez, B. R. Rost, B. Brokowski, B. Söhl-Kielczynski, A. Felies, M. W. Davis, C. Rosenmund, E. M. Jorgensen, *Nature* **2014**, *515*, 228–233.
[32] S. Takamori, M. Holt, K. Stenius, E. A. Lemke, M. Grønborg, D. Riedel, H. Urlaub, S. Schenck, B. Brügger, P. Ringler, et al., *Cell* **2006**, *127*, 831–846.
[33] F. Opazo, M. Levy, M. Byrom, C. Schäfer, C. Geisler, T. W. Groemer, A. D. Ellington, S. O. Rizzoli, *Nat. Methods* **2012**, *9*, 938–939.
[34] J. Ries, C. Kaplan, E. Platonova, H. Eghlidi, H. Ewers, *Nat. Methods* **2012**, *9*, 582–584.

Received: June 11, 2015
Revised: August 4, 2015
Published online: September 8, 2015

